Additive Manufacturing 36 (2020) 101487

Contents lists available at ScienceDirect

Additive Manufacturing

journal homepage: www.elsevier.com/locate/addma

Selective coaxial ink 3D printing for single-pass fabrication of smart elastomeric foam with embedded stretchable sensor

Jiawen Xu[a], Xinghao Zhang[a], Yu Liu[a,d,*], Yang Zhang[b,*], Heng-Yong Nie[c], Gaoyang Zhang[a], Weilian Gao[a]

[a] School of Mechanical Engineering, Jiangnan University, Wuxi, 214122, China
[b] Department of Mechanical Engineering, Technical University of Denmark, 2800 Kgs. Lyngby, Denmark
[c] Surface Science Western, The University of Western Ontario, London, N6A 3K7, Ontario, Canada
[d] Jiangsu Key Lab of Advanced Food Manufacturing Equipment and Technology, Jiangnan University, Wuxi, 214122, China

ARTICLE INFO

Keywords:
Smart elastomeric cellular material
Embedded strain sensor
Coaxial ink 3D printing
Selective deposition

ABSTRACT

Cellular materials are playing a critical role in a vast number of smart applications. Latest advances in additive manufacturing have catalyzed the structural metaproperties of the cellular materials. However, a major challenge remains for straightforward and rapid fabrication of smart cellular foams with embedded sensors while minimizing negative impacts on their mechanical performances. In this work, a selective coaxial ink 3D printing method is disclosed for manufacturing a smart elastomer cellular foam at a single pass, with its capability of precisely assigning a core–shell fiber segment as a strain sensor inside the cellular structure. Mechanical test results on these core–shell fiber segments point out that higher sensitivity can be obtained upon tension rather than compression. Therefore, in consideration of the effects of cellular structure i.e. face centered tetragonal (FCT) and simple cubic (SC), it is revealed that the FCT structure outperforms with a much higher strain sensitivity. By assigning different number of cellular layers and tuning the line spacing inside the cellular structure, the mechanical effects with embedding the sensor in the smart foam are assessed and increasing the line spacing might increase the sensitivity but will degrade the repeatability. In final, the stretching performance of the smart foam is studied, and its application is demonstrated.

1. Introduction

Dating back to around 1660s, Robert Hook ameliorated microscopes and carefully inspected the structure of corks, revealing the cellular structure resembling honeycomb. Such findings provided insights on how the cellular structure may influence overall properties and gradually inspire structure design of synthetic cellular foams that mimic their natural counterparts. Lately, the man-made natural cellular foams are endowed with extraordinary features, such as light weight [1–3], high compressibility [4–6], augmented specific surface area [7], enhanced buoyancy [8] and reduced thermal conductivity [9,10], which are desirable for various applications in machine damping [11], automobile and aircraft design [8], soft robots [12,13], and wearable electronics [14]. For preparation of these elastomeric cellular foams, the traditional methods via both physical [15–17] and chemical foaming [18–20], create stochastic pore distribution and result in unpredicted mechanical performance of the foam [21].

Recently, additive manufacturing (AM) has been developed as a powerful method for yields of orderly aligned and programmable cellular microstructures [22–26] across a variety of deployed materials, such as thermoplastics processed by FDM (Fused Deposition Modelling) [27,28], photocurable resin shaped up by SLA (Stereolithography Apparatus) [29] or DLP (Digital Light Processing) [30], metal powder stacked up by SLM (Selective Laser Melting) [31,32], and liquid-like material jetted by IJP (Ink Jetting Printing) [33,34]. As to the elastomeric materials (e.g., PDMS, PU), direct ink writing (DIW) AM technique is more compatible [35–38], e.g. fabrication of meta-foams with tunable density and stiffness [39,40], extraordinary durability [26] and high surface area [7]. Also, inside the elastomeric entities, selective deposition of sensing materials are being readily studied [41], through the principal innovations with developing interface-controlled DIW methodologies for rapid fabrication of gesture-sensible gloves [42,43], core-shell capacitive sensors [44] and somatosensitive finger [45]. With multi-material 3D digital jetting of functional inks [45–50], smart elastomeric cellular can be prepared which are sensitive to the resistance [41], piezoelectrics [4], magnetics [51], or temperature [52].

* Corresponding authors.
E-mail addresses: yuliu@jiangnan.edu.cn (Y. Liu), yaz@dtu.edu.dk (Y. Zhang).

https://doi.org/10.1016/j.addma.2020.101487
Received 12 April 2020; Received in revised form 8 July 2020; Accepted 22 July 2020
Available online 26 July 2020

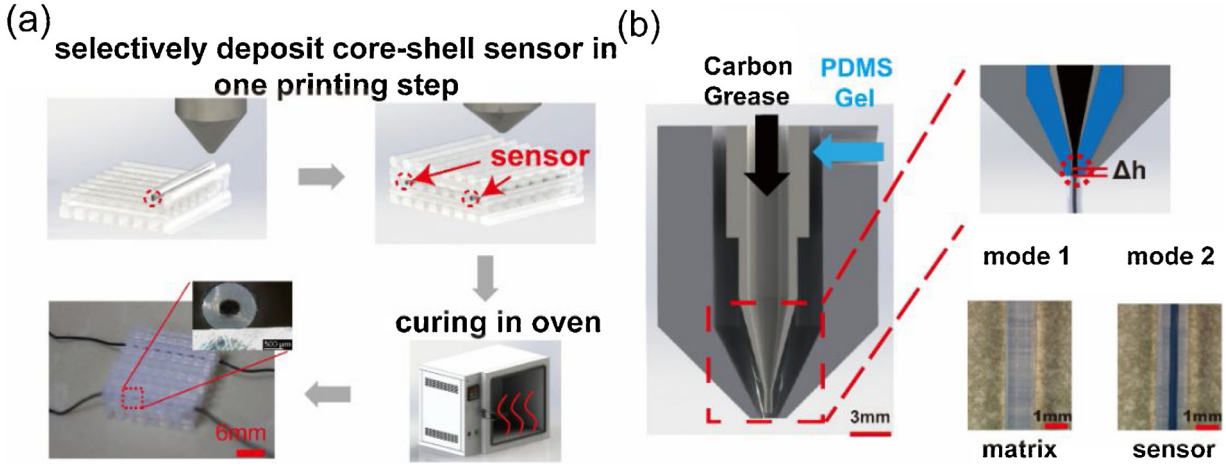

Fig. 1. (a) The whole procedure of preparation of elastic cellular materials, in which the embedded strain sensors were marked by dash circle; (b) Switching mode for producing PDMS matrix and senor.

And most of these efforts are requiring high credentials on ink designs, in regard to viscosities, moduli, interfacial wettability, and solidification e.g. via in-situ solvent evaporation [53,54] or post UV curing [55,56].

The above-mentioned development is difficult to be directly applied to embed sensor inside the cellular structure, in which a cell wall unit should be selectively decorated with sensing capability. The major challenges exist with decoupling the impacts from the functional fillers on ink rheological properties [36,52,57] and the structural integrity of the cellular material [11,58,59]. Despite several practices of implanting commercial strain sensors inside material matrix [60–62], the challenge lies in the sensor performance under large stretching and compressing inside the elastomeric cellular foam, as well as the relatively high cost and fabrication time [63–65]. Therefore, we are scoping the first attempt to develop selectively coaxial ink 3D printing for preparation of a smart elastomeric structure as shown in Fig. 1. According to our design, facile switching of core and shell inks extruded from a coaxial nozzle was controlled to produce the cellular matrix and then precisely allocate a core-shell fiber segment as the stretchable strain sensor. Therefore, both cellular structure and strain sensor are implemented by a single-pass fabrication. More details on this strategy will be discussed in following sections.

2. Materials and method

2.1. Materials systems

The elastomeric shell material was polydimethylsiloxane (PDMS, SE1700, Dow Corning Inc.) and prepared by mixing the base and catalyst at the weight ratio of 10:1. the PDMS was centrifuged for removing the trapped air bubbles. for constructing the elastomeric cellular structure and the shell of the embedded strain sensor. The core ink was carbon grease (Carbon Conductive Grease 846, MG Chemicals.) with electrical resistivity of 117Ω cm Prior to printing, both PDMS and carbon grease were loaded to 30 cc syringes (Nordson), and then centrifuged at 4000 rpm (for shell ink) and 2000 rpm (for core ink) for 2 min to remove bubbles. A glass slide was cleaned by 98 % alcohol and used as the substrate.

2.2. D printing of smart cellular foam

The whole schematic of our proposed manufacturing process is implemented on a home-built direct ink 3D writing system, which consists of a customized three – axis stage with a multi – axis motion controller. The stage's linear positioning accuracy was ± 5 μm. A coaxial ink extrusion module is equipped with a coaxial extruder, shell material reservoir, core material reservoir, and two separate ink supply modules. The coaxial extruder was made of stainless steel. Pneumatic dispenser was modified with electronic pressure regulating valve (SMC Corporation, Japan) for handling high viscosity inks with high pressure resolution 1 kPa. The standoff distance between the coaxial nozzle and the substrate was adjusted and maintained at about 1.3 mm. All moving trajectories for constructing the smart cellular foam were programmed in LabVIEW. In this paper, two typical cellular structures simple cubic (SC) and face centered tetragonal (FCT) are readily considered with significantly different mechanical performances [6,25].

Shown in Fig. 1, we started with extruding the PDMS shell ink by first turning off the purging pressure loaded on the core material (carbon grease ink) reservoir, and only printed the PDMS cell walls of the foam. When approaching the pre-set position for embedding the soft strain sensor, the purging pressure on the carbon grease ink was immediately switched on and the carbon ink was then extruded out in parallel with the PDMS ink to form the core–shell segment, which is also a part of the cell wall but play as a soft sensor. The whole process was recorded and can be viewed in the Video S2 (Supplement material). The accomplished sample was then sent for curing at the temperature of 120 °C for 0.5 h.

2.3. Simulations

The mechanical performances of SC and FCT structured foams with fiver layer design were simulated by FEA (finite element analysis) using ABAQUS software. In simulation, the PDMS shell diameter of the cellular foams was set as 1.30 mm with the line spacing of 3 mm and the height layer of 1.1 mm, respectively. Two thin plates assumed with high stiffness were assigned to sandwich the cellular structure, and the lower plate remained fixed. Then, a linear displacement was applied to move the upper plate downwards and therefore compress the cellular structures to a maximum strain of 0.5. Total 100 time intervals were calculated for getting the final results.

2.4. Characterizations

The rheological properties of PDMS and carbon grease were tested on a rheometer (DHR-2, TA instrument). The test fixture adopted is a cone plate with a cone angle of 2° and a diameter of 40 mm. The gap distance between cone and substrate is set as 59 μm. The relationship between viscosity and shear rate was obtained by the "Flow Sweep" where the range of shear rate is set as 0.01 s^{-1} to 1000 s^{-1}. The relationship between modulus and shear stress was attained by scanning

stress from 0 to 100 Pa with the oscillation frequency set at 1 Hz. All tests were conducted at 25 °C and 60 % relative humidity.

The dimensional data of the soft sensor and cellular foam were collected on an optical microscope (DVM6 A, Leica Microsystems GmbH). The cross sections of the coaxial wires are analyzed on a scanning electron microscope (SEM, HITACHI TM3030) at an acceleration voltage of 15 kV. A universal testing machine (QingJi QJ211, Shanghai) was used for compressive and tensile tests. The compressive speed and stretching speed were set as 5 and 50 mm/min, respectively. The resistance measurement was conducted using a digital multimeter (34465A, Keysight Inc.) while mechanical tests were performed with a sampling frequency of 2 Hz. After obtaining the complete cellular foam, we trimmed the foam and connected coaxial sensor using cooper wire and then dropped a little UV curable glue (SI 5091, Loctite) on cutting edge with UV curing for 5 min.

A Zeiss 3D X-ray microscope (Xradia 410 Versa, USA) was used to examine the structural details of 3D-printed cellular foams at a resolution of 1 μm. To image the 3D-printed samples, the X-ray source was operated at 60 kV and 133 μA (i.e., 8 W), with a low energy filter (LE5). Using a 0.4× objective, the source-sample and detector-sample distances are 42 and 150 mm, separately. With 4 camera binning, 1 s exposure time and 1601 projections, the scanning time for a sample was around an hour and the pixel size was 6.8 μm. In order to observe responses of the 3D-printed structure to pressures, a Deben microtest in-situ testing module (CT500, UK) was used to apply 20 N to compress samples whose sizes were 1.5 cm × 1.5 cm.

3. Results and discussion

3.1. Effects of printing parameters on core-shell sensor

In this proposed method, PDMS was selected as the shell ink for constituting the elastomeric cellular matrix. Conductive carbon grease served as piezo-resistive sensing material [28] of the soft embedded sensor, a sensing segment (also a minute portion of core-shell feature with precisely controlled segment length) being selectively deposited inside the cellular foam. In the experiments, such as deposition velocity, pressure, nozzle effect and wettability would influence the width of the printed PDMS shell [37,66,67]. However, the velocity and pressure were readily controlled in this study. To investigate their effects, we fixed the standoff distance between the end tip of extruder and substrate at about 1.3 mm. As shown in Fig. 2a, the higher deposition velocity and the lower air pressure could lead to smaller shell width, yet confronting with a higher risk of damaging the quality of the core-shell structure [68]. Therefore, the low limit on the shell width should be set at ~900 μm for the coaxial DIW.

By fixing the air purging pressure for PDMS shell ink at ~550 kPa, the decrease from 0 to 500 kPa on the air purging pressure for the core ink could change the core width from 0 to ~900 μm, shown in Fig. 2b. It was also noted that purging the core ink would require a lower limit of the air pressure at ~200 kPa, due to a slight height difference Δh (in Fig. 1b) between the two orifice ends of the coaxial nozzle. For investigating the electromechanical properties, we first fabricated core-shell samples with different core diameter, including ~270 μm, ~450 μm, ~560 μm, and ~1000 μm, maintaining same shell width of 1.3 mm and length of 110 mm. As shown in Fig. 3a and c, under the compressive load, the sensing segment presented degraded compressive strength and sensitivity with the increased core width, which also became less sensitive to the low strain range. For the stretching load along the core-shell segment, shown in Fig. 3b and d, greater resistance changes were observed in contrast rather than the compressive loading and therefore higher sensitivity. In summary, to achieve a higher sensitivity, the core-shell sensing segment if embedded in the cellular foam should be subjected to a tensile load rather than a compressive load, and this will help us to optimize structuring of the smart foam in next step. We also note that, when the soft segment underwent a large deformation, the nonlinear changing trends could be attributed to the net effects of constriction resistance, tunneling resistance and intrinsic filler resistance that are caused by the change of fillers' volume fracture in a nonlinear form [46].

3.2. Compressive performances of smart foams

For two typical cellular structures SC and FCT [25], the effects of the different layer numbers i.e. five and nine on the compressive performances were studied. For simplifying the investigation, the sensing segments were selectively deposited at the middle layer i.e. 3rd and 5th layer, respectively. All sample had the same cubic size of 25 mm, and the embedded sensors has the core width of ~300 μm. Under compression, the cellular foam experiences linear elastic, plateau and densification stages [6]. For the traditional cellular foam (t-cf) with only 5 layers, it reached the densification stage at a given engineering strain of 0.15, shown in Fig. 4b. Under the same load, the smart cellular foam (s-cf) with an embedded strain sensor showed degraded mechanical strength because the flowability of carbon ink impacts the effective stiffness of the smart foam. Nevertheless, for the 9-layer t-cf and s-cf, their mechanical curves did not show much difference, and the smart cellular foam with more layer number can exhibit robustness.

In consideration of the impacts of different cellular structures i.e. SC and FCT, the same geometric properties were obtained with PDMS shell width of ~1.3 mm, core width of ~500 μm, spacing of 3 mm, and cubic size of ~20 mm × 20 mm × 5.5 mm. The sensor was embedded in the

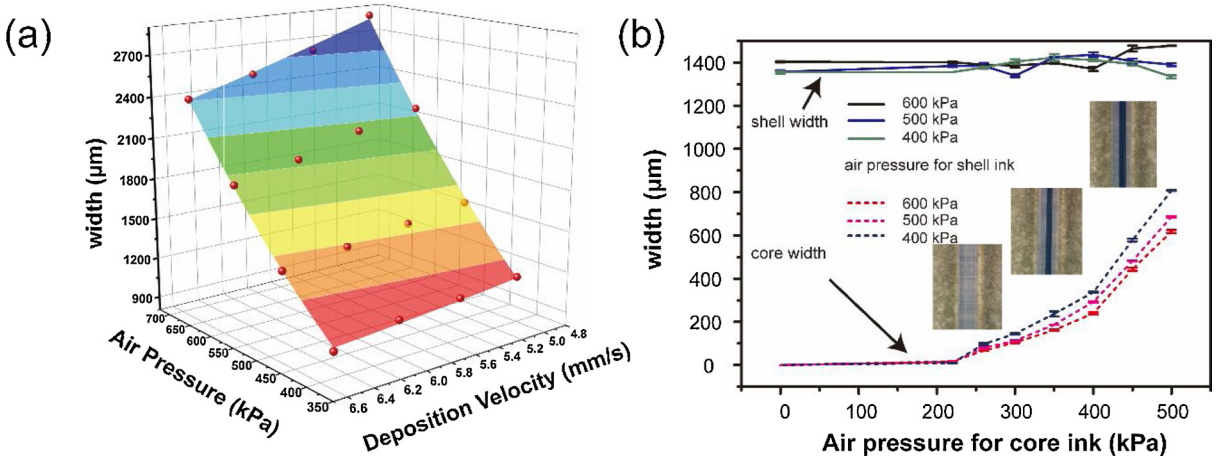

Fig. 2. (a) The PDMS shell width as the function of air purging pressure and deposition velocity; (b) The relationship between the core width and the air purging pressure.

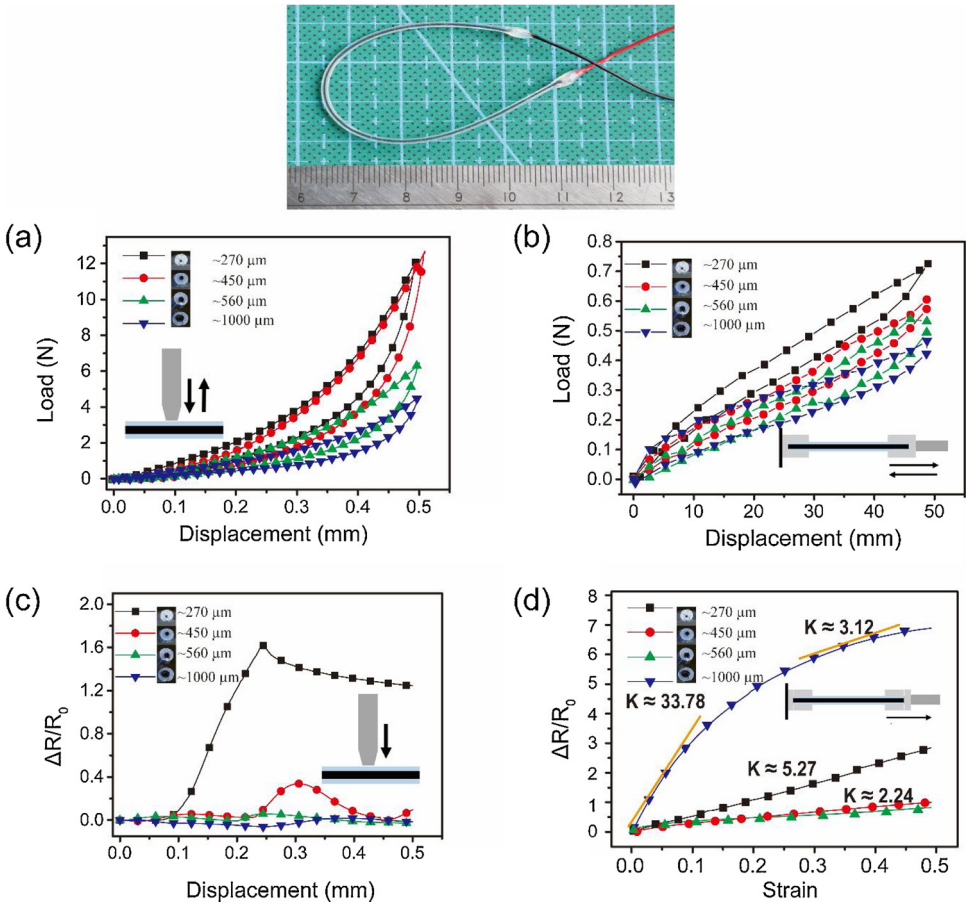

Fig. 3. Mechanical testing results of printed core–shell sensing segments: (a) force – displacement curves from the compressive experiments; (b) force – displacement curves from the tensile experiments, (c) resistance change with the compressive displacement; and (d) the resistance change with the tensile strain.

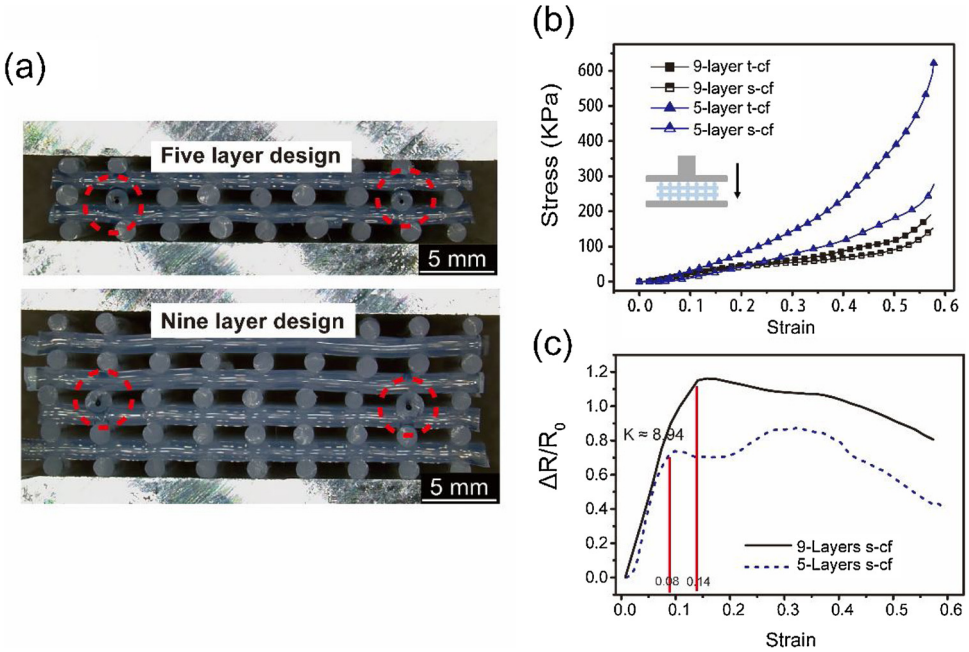

Fig. 4. (a) Cross-section views of a 5- and 9-layer smart cellular foams with embedded sensors as marked by dash circles; (b) strain-stress curves and (c) resistance change as a function of strain for simple cubic structures with different number of layers.

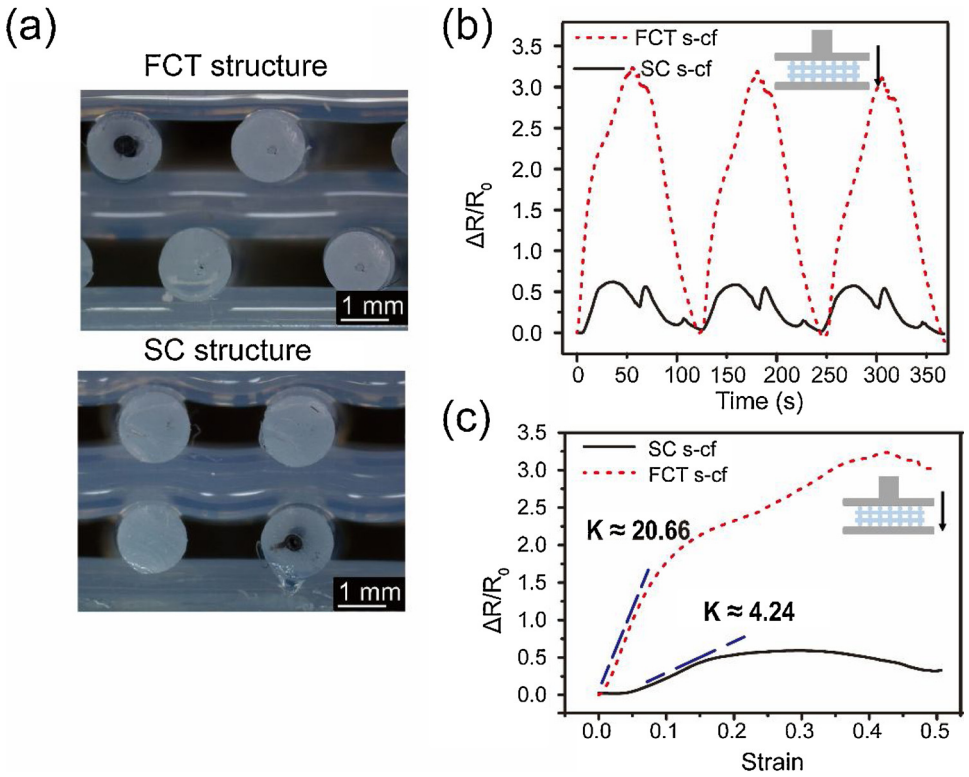

Fig. 5. (a) Cross-section views of the FCT and SC structured foams with embedded strain sensors; (b) and (c) the resistance variation rate as function of strain.

middle of 3rd layer. The same printing parameters include deposition velocity of 8 mm/s, layer height of 1.1 mm, air pressure of 600 kPa (shell) and 450 kPa (core). The results shown in Fig. 5b show that the embedded sensors for both SC and FCT structures exhibited high repeatability and the FCT owns higher response amplitude. Furthermore, the resistance of the senor for FCT s-cf changed almost linearly with the strain and approached a high sensitivity of ~20.66, while the sensor in SC s-cf only exhibited a sensitivity of ~4.24 with a narrow linear range.

To understand these different behaviors, both finite elements (FE) simulation and micro-CT imaging on the SC and FCT s-cf were performed. As shown in Fig. 6a, under the same compressive strain, the struts in the FCT foam experienced a dominant stretching provided by compressing the staggered strands adjacent to the strain sensor, rather than a compressing seen in SC at positions where the upper and lower struts are aligned vertically. This simulation is verified by compressing the SC and FCT samples and imaging their 3D structures using a micro-computed tomography (micro-CT) technique [64], which reveals the 3D structure of an object. Shown in Fig. 6b are 3D images rendered from the micro-CT data with virtual sectioning across and along sensor segement. The two samples were compressed under the same applied force of 20 N, or compressive stress of 89 kPa, resulting in a strain of 0.38 and 0.51 for the SC foam (left) and FCT foam (right), respectively. For the SC foam under compression, the struts sandwiching the sensor clamped. By contrast, the staggered strands from the top and bottom of the sensor stretched themselves significantly via a wave-like deformation.

Based on the conclusion above, FCT structure with higher sensitivity was chosen for studying the effect from the line spacing *d*, shown in Fig. 7a. We fabricated three 5-layer samples for each different line spacing of 2.0 mm, 2.5 mm and 3.0 mm, by maintaining the same sample size of 20 mm × 20 mm × 5.5 mm, the shell width of 1.3 mm, and the sensor embedded at the 3rd layer. All samples were compressed in a linear range by loading from 0 N to 10 N. From the results in Fig. 7a, it was first noted that the samples with the same design demonstrated force sensing variance, due to the coupled impacts from the uniformities of shell width, core width, spacing and distribution of the core ink (SEM image in Fig. 7c). However, this variance is acceptable in contrast with that from the impacts of the line spacing. Therefore, for controlling the sensing repeatability, line spacing should be readily fine-tuned.

3.3. Stretching performances of elastic foams

In the fields of flexible electronics, stretching applications are attracting the community. Therefore, stretching performance of the developed smart foams was also studied in this work. As shown in Fig. 8a, a new 5-layered FCT sample with the size of 20 mm × 60 mm × 5.5 mm was fabricated with the shell width of 1.3 mm and the core width of 0.65 mm. The reason of using a length of 60 mm rather than 20 mm in previous studies was to provide an enough area for migrating the possible impacts from the clipping during the stretching. The FCT structure with higher sensitivity was selected with the spacing set as 3 mm. From the results in Fig. 8b, the smart foam with the embedded sensor displayed very high repeatability with strain up to 100 %. And the Fig. 8c clearly show the substantial resistance change with the sensitivity up to ~25 when the sensor was stretched within the strain up to 0.4. This sensitivity value is at the same order of and slightly higher than the sensitivity of the FCT structure. We could conclude that during stretching the FCT structured smart foam undertook both of compressive and tensile deformation. As a final, we fabricated a cellular finger ring, with three embedded sensors located at top, right and left sides of the finger. The motion of fisting generated three signals from these sensors, and a major change happened with the top sensor as expected. And the two side sensors show slightly different signals. We will expect that the developed smart cellular foam could be used as high-performance wearable sensor with preferred breathability, light weight and stretchability at multiple scales.

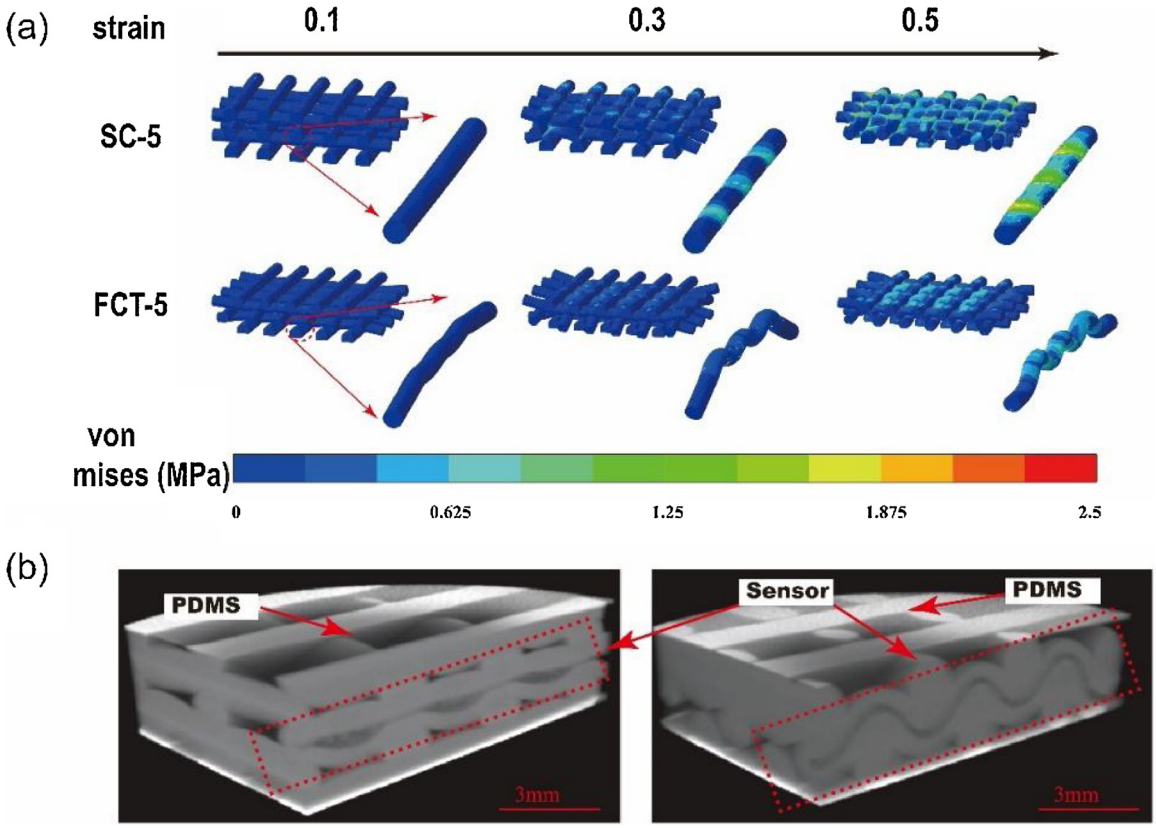

Fig. 6. (a) Simulations of smart foams with different structure designs under a strain range from 0 to 0.5; (b) 3D images rendered from micro-CT data with virtual cross sections showing the deformation of the embedded sensor at a compressive stress of 89 kPa, resulting in a strain of 0.38 for the SC foam (left) and 0.51 for the FCT foam (right).

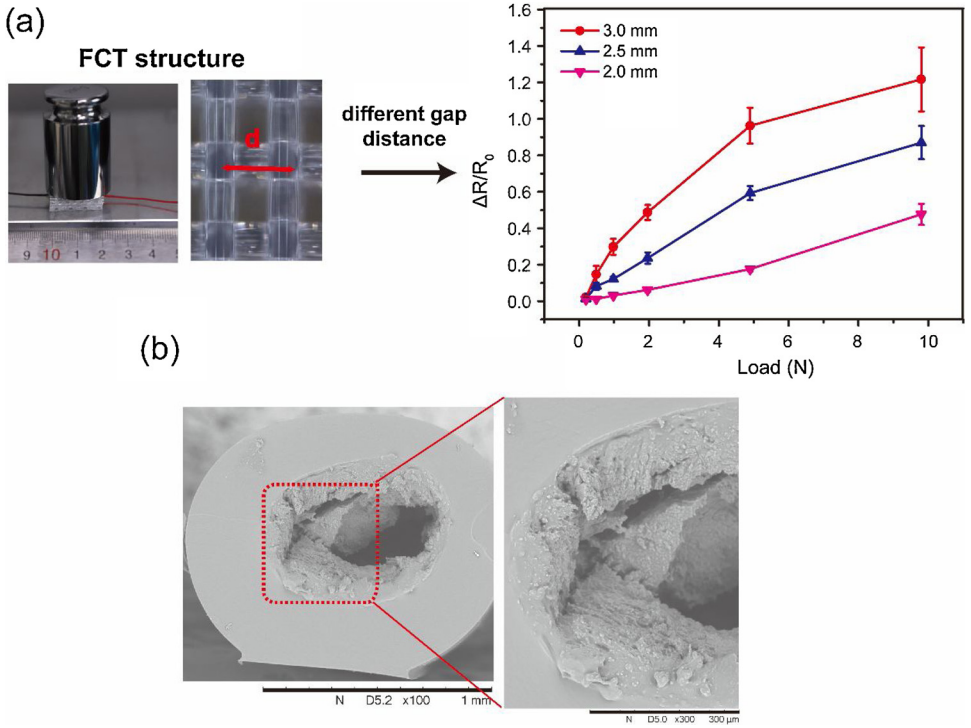

Fig. 7. (a) The measured curves of the relative resistance ratios on FCT samples with different force loads; (b) SEM image of cross-sectional view of core-shell sensor embedded in smart foam.

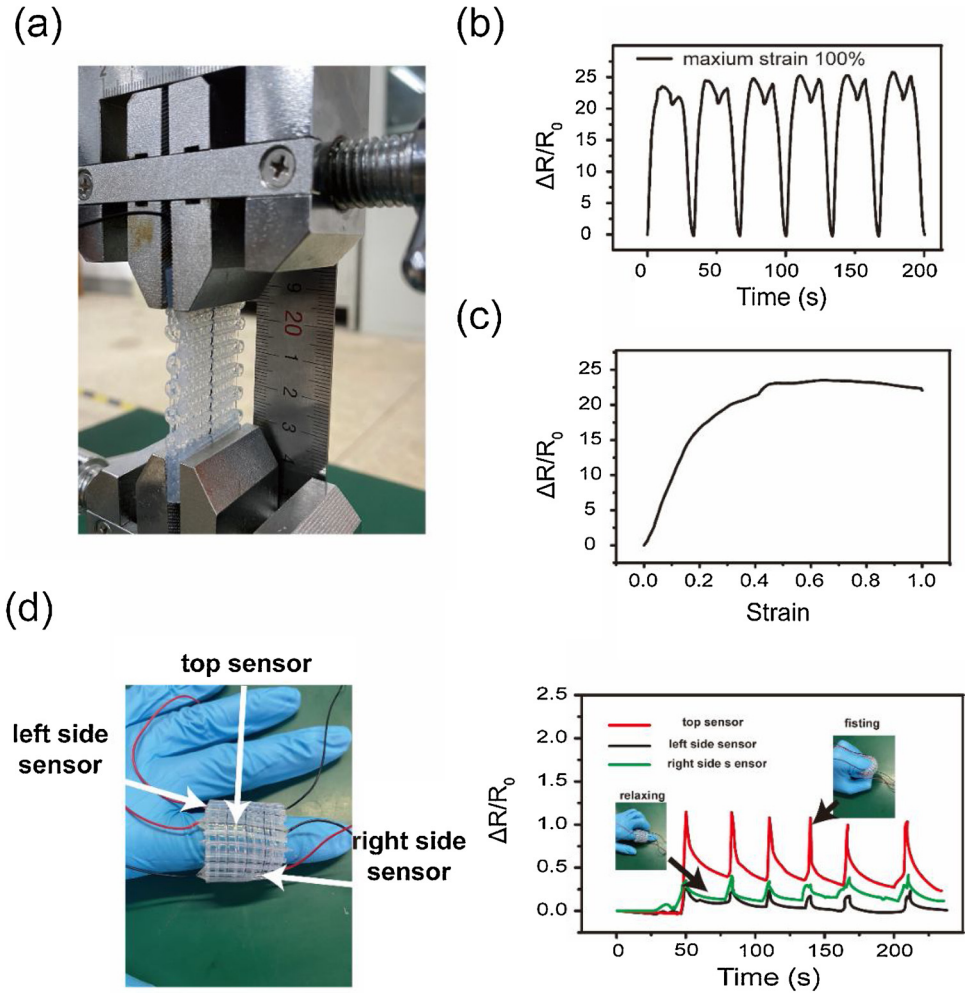

Fig. 8. (a) Setup for stretching tests; (b) The changes of the resistance ratios with the stretching elongation up to 100 %; (c) The changes of the resistance ratios with different strains; (d) Smart cellular foam for sensing finger motions.

4. Conclusion

In summary, we report a facile method for fabricating smart elastomeric cellular foams with embedded strain sensors. To our best knowledge, it is the first attempt dedicated to the development of advanced cellular materials with controlled embedment of sensors regarding their positions, sensitivities, repeatability and size effects. With a preferable embodiment of the sensor in FCT cellular design, high sensitivity has been attained by enhancing its stretching response rather than the compressing response, which can be further optimized in future works. The method and its derivatives would be attractive for manufacturing and advancing novel functional components via 3D printing. By incorporating the sensing function, the smart elastomeric foam can implement many practical applications requiring a sensitive stress feedback, such as robotic gripper for picking up fragile objects, wearable electronics for human health monitoring, and smart meta-cushion for precision packaging.

Declaration of Competing Interests

The authors declare that they have no known competing financial interests or personal relationships that could have appeared to influence the work reported in this paper.

CRediT authorship contribution statement

Jiawen Xu: Writing - original draft, Methodology, Conceptualization, Investigation, Supervision, Funding acquisition. **Xinghao Zhang:** Writing - original draft, Methodology, Investigation. **Yu Liu:** Writing - original draft, Methodology, Conceptualization, Investigation, Supervision, Funding acquisition. **Yang Zhang:** Writing - original draft, Methodology, Conceptualization, Supervision. **Heng-Yong Nie:** Writing - review & editing, Supervision. **Gaoyang Zhang:** Investigation. **Weilian Gao:** Investigation, Writing - review & editing.

Acknowledgments

This work is financially supported by National Natural Science Foundation of China (Grant No. 51875253), the Experience Design Frontier Methodology and Technology Innovation Research Project (111Project, No. B18027) and Postgraduate Research and Practice Innovation Program of Jiangsu Province KYCX20_1830.

Appendix A. Supplementary data

Supplementary material related to this article can be found, in the online version, at doi:https://doi.org/10.1016/j.addma.2020.101487.

References

[1] Y. Qin, Q. Peng, Y. Ding, Z. Lin, C. Wang, Y. Li, F. Xu, J. Li, Y. Yuan, X. He, Lightweight, superelastic, and mechanically flexible graphene/polyimide nanocomposite foam for strain sensor application, ACS Nano 9 (2015) 8933–8941.

[2] P.G. Dixon, J.T. Muth, X. Xiao, M.A. Skylar-Scott, J.A. Lewis, L.J. Gibson, 3D printed structures for modeling the Young's modulus of bamboo parenchyma, Acta Biomater. 68 (2018) 90–98.

[3] J.M. McCracken, A. Badea, M.E. Kandel, A.S. Gladman, D.J. Wetzel, G. Popescu, J.A. Lewis, R.G. Nuzzo, Programming mechanical and physicochemical properties of 3D hydrogel cellular microcultures via direct ink writing, Adv. Healthc. Mater. 5 (2016) 1025–1039.

[4] N. Frioui, A. Bezazi, C. Remillat, F. Scarpa, J.P. Gomez, Viscoelastic and compression fatigue properties of closed cell PVDF foam, Mech. Mater. 42 (2010) 189–195.

[5] S. Liang, Y. Li, J. Yang, J. Zhang, C. He, Y. Liu, X. Zhou, 3D stretchable, compressible, and highly conductive metal-coated polydimethylsiloxane sponges, Adv. Mater. Technol. 1 (2016).

[6] X. Zhu, Y. Chen, Y. Liu, Y. Deng, C. Tang, W. Gao, J. Mei, J. Zhao, T. Liu, J. Yang, Additive manufacturing of elastomeric foam with cell unit design for broadening compressive stress plateau, Rapid Prototyp. J. 24 (2018) 1579–1585.

[7] J. Zhao, Y. Zhang, X. Zhao, R. Wang, J. Xie, C. Yang, J. Wang, Q. Zhang, L. Li, C. Lu, Y. Yao, Direct ink writing of adjustable electrochemical energy storage device with high gravimetric energy densities, Adv. Funct. Mater. 29 (2019).

[8] D.S. Schwartz, Porous and Cellular Materials for Structural Applications, Materials Research Society, Warrendale, Pennsylvania, USA, 1998.

[9] X. Xu, Q. Zhang, M. Hao, Y. Hu, Z. Lin, L. Peng, T. Wang, X. Ren, C. Wang, Z. Zhao, Double-negative-index ceramic aerogels for thermal superinsulation, Science 363 (2019) 723–727.

[10] A. Öchsner, G.E. Murch, M.J. de Lemos, Cellular and Porous Materials: Thermal Properties Simulation and Prediction, John Wiley & Sons, Federal Republic of Germany, 2008.

[11] B.C. Mac Murray, X. An, S.S. Robinson, I.M. van Meerbeek, K.W. O'Brien, H. Zhao, R.F. Shepherd, Poroelastic foams for simple fabrication of complex soft robots, Adv. Mater. 27 (2015) 6334–6340.

[12] S. Janbaz, F.S. Robbert, M.J. Mirzaali, A.A. Zadpoor, Mater. Horiz. 6 (2019) 1138–1147.

[13] M. Kaur, W.S. Kim, Toward a smart compliant robotic gripper equipped with 3D-designed cellular fingers, Adv. Intell. Syst. 1 (2019).

[14] X. Wu, K. Hou, J. Huang, J. Wang, S. Yang, Graphene-based cellular materials with extremely low density and high pressure sensitivity based on self-assembled graphene oxide liquid crystals, J. Mater. Chem. C 6 (2018) 8717–8725.

[15] R. Verdejo, C. Saiz-Arroyo, J. Carretero-Gonzalez, F. Barroso-Bujans, M.A. Rodriguez-Perez, M.A. Lopez-Manchado, Physical properties of silicone foams filled with carbon nanotubes and functionalized graphene sheets, Eur. Polym. J. 44 (2008) 2790–2797.

[16] L. Li, B. Li, L. Wu, X. Zhao, J. Zhang, Magnetic, superhydrophobic and durable silicone sponges and their applications in removal of organic pollutants from water, Chem. Commun. (Camb.) 50 (2014) 7831–7833.

[17] O. Voronina, M. Wegener, W. Wirges, R. Gerhard, L. Zirkel, H. Münstedt, Physical foaming of fluorinated ethylene-propylene (FEP) copolymers in supercritical carbon dioxide: single-film fluoropolymer piezoelectrets, Appl. Phys. A 90 (2007) 615–618.

[18] S.-T. Lee, N.S. Ramesh, Polymeric Foams: Mechanisms and Materials, Materials Research Society, Warrendale, PA 15086, USA, 2004.

[19] X. Zhao, L. Li, B. Li, J. Zhang, A. Wang, Durable superhydrophobic/superoleophilic PDMS sponges and their applications in selective oil absorption and in plugging oil leakages, J. Mater. Chem. A 2 (2014) 18281–18287.

[20] S.J. Choi, T.H. Kwon, H. Im, D.I. Moon, D.J. Baek, M.L. Seol, J.P. Duarte, Y.K. Choi, A polydimethylsiloxane (PDMS) sponge for the selective absorption of oil from water, ACS Appl. Mater. Interfaces 3 (2011) 4552–4556.

[21] S. Yuan, C.K. Chua, K. Zhou, 3D-printed mechanical metamaterials with high energy absorption, Adv. Mater. Technol. 4 (2019) 1800419.

[22] I. Gibson, D.W. Rosen, B. Stucker, Additive Manufacturing Technologies, Springer, New York, Heidelberg, Dordrecht, London, USA, 2014.

[23] A. Clausen, F. Wang, J.S. Jensen, O. Sigmund, J.A. Lewis, Topology optimized architectures with programmable Poisson's ratio over large deformations, Adv. Mater. 27 (2015) 5523–5527.

[24] J. Mueller, J.R. Raney, K. Shea, J.A. Lewis, Architected lattices with high stiffness and toughness via multicore-shell 3D printing, Adv. Mater. 30 (2018) e1705001.

[25] E.B. Duoss, T.H. Weisgraber, K. Hearon, C. Zhu, W. Small, T.R. Metz, J.J. Vericella, H.D. Barth, J.D. Kuntz, R.S. Maxwell, C.M. Spadaccini, T.S. Wilson, Three-dimensional printing of elastomeric, cellular architectures with negative stiffness, Adv. Funct. Mater. 24 (2014) 4905–4913.

[26] A. Maiti, W. Small, J.P. Lewicki, T.H. Weisgraber, E.B. Duoss, S.C. Chinn, M.A. Pearson, C.M. Spadaccini, R.S. Maxwell, T.S. Wilson, 3D printed cellular solid outperforms traditional stochastic foam in long-term mechanical response, Sci. Rep. 6 (2016) 24871.

[27] H. Ota, S. Emaminejad, Y. Gao, A. Zhao, E. Wu, S. Challa, K. Chen, H.M. Fahad, A.K. Jha, D. Kiriya, W. Gao, H. Shiraki, K. Morioka, A.R. Ferguson, K.E. Healy, R.W. Davis, A. Javey, Application of 3D printing for smart objects with embedded electronic sensors and systems, Adv. Mater. Technol. 1 (1) (2016) 1600013.

[28] S. Dul, L. Fambri, A. Pegoretti, Fused deposition modelling with ABS–graphene nanocomposites, Composites A 85 (2016) 181–191.

[29] J. Wang, A. Goyanes, S. Gaisford, A.W. Basit, Stereolithographic (SLA) 3D printing of oral modified-release dosage forms, Int. J. Pharm. 503 (2016) 207–212.

[30] Q. Mu, L. Wang, C.K. Dunn, X. Kuang, F. Duan, Z. Zhang, H.J. Qi, T. Wang, Digital light processing 3D printing of conductive complex structures, Addit. Manuf. 18 (2017) 74–83.

[31] Y. Kim, E. Stoykova, H. Kang, S. Hong, J. Park, J. Park, J. Hong, Seamless full color holographic printing method based on spatial partitioning of SLM, Opt. Express 23 (2015) 172–182.

[32] Z. Sun, X. Tan, S.B. Tor, W.Y. Yeong, Selective laser melting of stainless steel 316L with low porosity and high build rates, Mater. Des. 104 (2016) 197–204.

[33] S. Agarwala, G.L. Goh, Y.L. Yap, G.D. Goh, H. Yu, W.Y. Yeong, T. Tran, Development of bendable strain sensor with embedded microchannels using 3D printing, Sens. Actuators A: Phys. 263 (2017) 593–599.

[34] W. Ye, J. Lin, R. Borrego, D. Chen, A. Sotto, P. Luis, M. Liu, S. Zhao, C.Y. Tang, B. Van der Bruggen, Advanced desalination of dye/NaCl mixtures by a loose nanofiltration membrane for digital ink-jet printing, Sep. Purif. Technol. 197 (2018) 27–35.

[35] M.A. Skylar-Scott, J. Mueller, C.W. Visser, J.A. Lewis, Voxelated soft matter via multimaterial multinozzle 3D printing, Nature 575 (2019) 330–335.

[36] L.Y. Zhou, Q. Gao, J.Z. Fu, Q.Y. Chen, J.P. Zhu, Y. Sun, Y. He, Multimaterial 3D printing of highly stretchable silicone elastomers, ACS Appl. Mater. Interfaces 11 (2019) 23573–23583.

[37] J.A. Lewis, Direct ink writing of 3D functional materials, Adv. Funct. Mater. 16 (2006) 2193–2204.

[38] R.L. Truby, J.A. Lewis, Printing soft matter in three dimensions, Nature 540 (2016) 371.

[39] M.M. Durban, J.M. Lenhardt, A.S. Wu, Wt. Small, T.M. Bryson, L. Perez-Perez, D.T. Nguyen, S. Gammon, J.E. Smay, E.B. Duoss, J.P. Lewicki, T.S. Wilson, Custom 3D printable silicones with tunable stiffness, Macromol. Rapid Commun. 39 (2018).

[40] Q. Chen, P.-F. Cao, R.C. Advincula, Mechanically robust, ultraelastic hierarchical foam with tunable properties via 3D printing, Adv. Funct. Mater. 28 (2018).

[41] P.F. Flowers, C. Reyes, S. Ye, M.J. Kim, B.J. Wiley, 3D printing electronic components and circuits with conductive thermoplastic filament, Addit. Manuf. 18 (2017) 156–163.

[42] J.T. Muth, D.M. Vogt, R.L. Truby, Y. Menguc, D.B. Kolesky, R.J. Wood, J.A. Lewis, Embedded 3D printing of strain sensors within highly stretchable elastomers, Adv. Mater. 26 (2014) 6307–6312.

[43] P. Millereau, E. Ducrot, J.M. Clough, M.E. Wiseman, H.R. Brown, R.P. Sijbesma, C. Creton, Mechanics of elastomeric molecular composites, Proc. Natl. Acad. Sci. U. S. A. 115 (2018) 9110–9115.

[44] A. Frutiger, J.T. Muth, D.M. Vogt, Y. Menguc, A. Campo, A.D. Valentine, C.J. Walsh, J.A. Lewis, Capacitive soft strain sensors via multicore-shell fiber printing, Adv. Mater. 27 (2015) 2440–2446.

[45] R.L. Truby, M. Wehner, A.K. Grosskopf, D.M. Vogt, S.G.M. Uzel, R.J. Wood, J.A. Lewis, Soft somatosensitive actuators via embedded 3D printing, Adv. Mater. 30 (2018) e1706383.

[46] J.R. Raney, B.G. Compton, J. Mueller, T.J. Ober, K. Shea, J.A. Lewis, Rotational 3D printing of damage-tolerant composites with programmable mechanics, Proc. Natl. Acad. Sci. U. S. A. 115 (2018) 1198–1203.

[47] N. Zhou, C. Liu, J.A. Lewis, D. Ham, Gigahertz electromagnetic structures via direct ink writing for radio-frequency oscillator and transmitter applications, Adv. Mater. 29 (2017) 1605198.

[48] E.B. Secor, B.Y. Ahn, T.Z. Gao, J.A. Lewis, M.C. Hersam, Rapid and versatile photonic annealing of graphene inks for flexible printed electronics, Adv. Mater. 27 (2015) 6683–6688.

[49] S. Xu, D.M. Vogt, W.H. Hsu, J. Osborne, T. Walsh, J.R. Foster, S.K. Sullivan, V.C. Smith, A. Rousing, E.C. Goldfield, R.J. Wood, Biocompatible Soft fluidic strain and force sensors for wearable devices, Adv. Funct. Mater. 29 (2019) 1807058.

[50] J.U. Lind, T.A. Busbee, A.D. Valentine, F.S. Pasqualini, H. Yuan, M. Yadid, S.J. Park, A. Kotikian, A.P. Nesmith, P.H. Campbell, J.J. Vlassak, J.A. Lewis, K.K. Parker, Instrumented cardiac microphysiological devices via multimaterial three-dimensional printing, Nat. Mater. 16 (2017) 303–308.

[51] R. Zhao, Y. Kim, S.A. Chester, P. Sharma, X. Zhao, Mechanics of hard-magnetic soft materials, J. Mech. Phys. Solids 124 (2019) 244–263.

[52] Z. Wang, W. Gao, Q. Zhang, K. Zheng, J. Xu, W. Xu, E. Shang, J. Jiang, J. Zhang, Y. Liu, 3D-printed graphene/polydimethylsiloxane composites for stretchable and strain-insensitive temperature sensors, ACS Appl. Mater. Interfaces 11 (2019) 1344–1352.

[53] J.H. Kim, S. Lee, M. Wajahat, H. Jeong, W.S. Chang, H.J. Jeong, J.R. Yang, J.T. Kim, S.K. Seol, Three-dimensional printing of highly conductive carbon nanotube microarchitectures with fluid ink, ACS Nano 10 (2016) 8879–8887.

[54] S. Lee, J.H. Kim, M. Wajahat, H. Jeong, W.S. Chang, S.H. Cho, J.T. Kim, S.K. Seol, Three-dimensional printing of silver microarchitectures using newtonian nanoparticle inks, ACS Appl. Mater. Interfaces 9 (2017) 18918–18924.

[55] Y. Guo, J. Xu, C. Yan, Y. Chen, X. Zhang, X. Jia, Y. Liu, X. Wang, F. Zhou, Direct ink writing of high performance architectured polyimides with low dimensional shrinkage, Adv. Eng. Mater. 21 (2019) 1801314.

[56] C.W. Visser, D.N. Amato, J. Mueller, J.A. Lewis, Architected polymer foams via direct bubble writing, Adv. Mater. 31 (2019) 1904668.

[57] A.S. Wu, W. Small Iv, T.M. Bryson, E. Cheng, T.R. Metz, S.E. Schulze, E.B. Duoss, T.S. Wilson, 3D printed silicones with shape memory, Sci. Rep. 7 (2017) 4664.

[58] A. Nieto, B. Boesl, A. Agarwal, Multi-scale intrinsic deformation mechanisms of 3D graphene foam, Carbon 85 (2015) 299–308.

[59] B. Oh, Y.G. Park, H. Jung, S. Ji, W.H. Cheong, J. Cheon, W. Lee, J.U. Park, Untethered Soft robotics with fully integrated wireless sensing and actuating systems for somatosensory and respiratory functions, Soft Robot. (2020), https://doi.org/10.1089/soro.2019.0066.

[60] A.D. Valentine, T.A. Busbee, J.W. Boley, J.R. Raney, A. Chortos, A. Kotikian, J.D. Berrigan, M.F. Durstock, J.A. Lewis, Hybrid 3D printing of soft electronics, Adv.

Mater. 29 (2017) 1703817.
[61] H. Shim, K. Sim, F. Ershad, P. Yang, A. Thukral, Z. Rao, H.J. Kim, Y. Liu, X. Wang, G. Gu, L. Gao, X. Wang, Y. Chai, C. Yu, Stretchable elastic synaptic transistors for neurologically integrated soft engineering systems, Sci. Adv. 5 (2019) eaax4961.
[62] R.Y. Tay, H. Li, J. Lin, H. Wang, J.S.K. Lim, S. Chen, W.L. Leong, S.H. Tsang, E.H.T. Teo, Lightweight, superelastic boron nitride/polydimethylsiloxane foam as air dielectric substitute for multifunctional capacitive sensor applications, Adv. Funct. Mater. 30 (2020) 1909604.
[63] E.L. White, J.C. Case, R.K. Kramer, Multi-mode strain and curvature sensors for soft robotic applications, Sens. Actuators A: Phys. 253 (2017) 188–197.
[64] H. Thienpont, J. Missinne, P. Van Daele, G. Van Steenberge, B. Van Hoe, J. Mohr, H. Zappe, E. Bosman, C. Debaes, J. Van Erps, C. Yan, E. Ferraris, P. Van Daele, J. Vanfleteren, D. Reynaerts, High density optical pressure sensor foil based on arrays of crossing flexible waveguides, Proc. Micro Opt. 2010 (2010) 77161G.
[65] P.A. Xu, A. Mishra, H. Bai, C. Aubin, L. Zullo, R. Shepherd, Optical lace for synthetic afferent neural networks, Sci. Robot. 4 (2019) eaaw6304.
[66] X. Zhu, Y. Chen, Y. Liu, C. Tang, T. Liu, J. Mei, W. Gao, J. Yang, Revisiting effects of microarchitecture on mechanics of elastomeric cellular materials, Appl. Phys. A 125 (2019) 247.
[67] H. Yuk, X. Zhao, A new 3D printing strategy by harnessing deformation, instability, and fracture of viscoelastic inks, Adv. Mater. 30 (2018) 1704028.
[68] H.-l. Yan, Y.-q. Chen, Y.-q. Deng, L.-l. Zhang, X. Hong, W.-m. Lau, J. Mei, D. Hui, H. Yan, Y. Liu, Coaxial printing method for directly writing stretchable cable as strain sensor, Appl. Phys. Lett. 109 (2016) 082502.